COMPUTATIONAL FLUID DYNAMICAL ANALYSIS OF COMPLEX INTERNAL FLOWS IN CENTRIFUGAL PUMPS

by

Paul Cooper

Director, Advanced Technology

Edward Graf

Senior Engineering Consultant

and

Timothy Luce

Analytical Engineer

Ingersoll-Dresser Pump Company

Phillipsburg, New Jersey

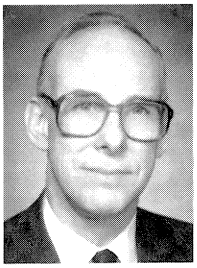

Paul Cooper is director of Advanced Technology for Ingersoll-Dresser Pump Company, Phillipsburg, New Jersey. His responsibilities are the development of new pump products along with the hydraulic and acoustical improvement of centrifugal pumps.

Dr. Cooper joined Ingersoll-Rand's research center in Princeton in 1977, where he conducted research on pumps and turbines. Prior to that, he had hydraulic design responsibility for aircraft fuel and oil field pumps at TRW, Incorporated.

Dr. Cooper received a B.S. degree in Mechanical Engineering (1957) from Drexel University, an M.S. degree (1959) from Massachusetts Institute of Technology, and a Ph.D. (1972) from Case Western Reserve University. Dr. Cooper is an ASME Fellow, having served as chairman of the ASME Fluids Engineering Division. He recently received ASME's Henry R. Worthington Medal for achievement in the field of pumping machinery.

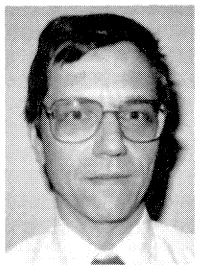

Edward Graf is a Senior Engineering Consultant in the areas of fluid dynamics and computational fluid dynamics for the Advanced Technology Group of Ingersoll-Dresser Pumps, Phillipsburg, New Jersey. His primary responsibilities are adapting sophisticated codes to the hydraulic and acoustic design and analysis of high energy industrial pumps and super-quiet pumps for Navy submarine applications.

Mr. Graf joined Ingersoll-Rand with the Turbo Division in 1981, during which time he had primary responsibility for the aerodynamic design of all advanced axial flow turbomachinery, including compressors, power turbines, and hot gas expanders.

Previously, Mr. Graf was employed as a Senior Engineer with the Westinghouse Electric Corporation with responsibility for the aerodynamic design of turbomachinery for specialized applications.

Mr. Graf received his B.S.M.E. degree at the University of Pennsylvania and his M.S.M.E. at the California Institute of Technology. He is presently pursuing a doctorate in the field of two-phase flows at Lehigh University. He is a member of the ASME and a licensed Professional Engineer in the State of Pennsylvania.

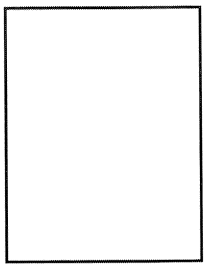

Timothy Luce is an Analytical Engineer with the Advanced Technology Group of Ingersoll-Dresser Pump Company, Phillipsburg, New Jersey. His responsibilities include both the acoustic and computational fluid dynamic analysis of pumps for industrial and Navy submarine applications.

Mr. Luce joined the Engineered Pump Division of Ingersoll-Rand in 1987 with the responsibility for acoustic analysis and optimization of Navy submarine pumps. Strong fluid dynamically induced acoustic sources led to his recent computational fluid dynamics work to identify and modify those sources within the pump.

Mr. Luce received his B.A. degree in Physics from Mansfield University of Pennsylvania and his M.S. degree in Acoustics from Pennsylvania State University. He is a member of the Institute of Noise Control Engineering.

ABSTRACT

A commercial computational fluid dynamics (CFD) computer code was employed to compute the flow field from 105 percent down to 21 percent of the 4525 gpm BEP flowrate of a 1785 rpm, 1500 specific speed impeller of 13,000 suction specific speed. Suction and discharge recirculation were both computed, and the results agreed in all details that have also been observed experimentally. The insights gained from these computations led to the design and construction of a new impeller aimed at smoother minimum flow operation. The same code was then applied to the computation of the highly three-dimensional flowfield of the diffusing crossover of a 325 gpm, 3580 rpm, 900 to 1000 specific speed multistage volute pump. Flow distortions produced by this crossover were computed at the outlet to the impeller of the succeeding stage, and the effects on performance were estimated. Candidate improvements to the crossover were evaluated with the same code, illustrating the utility of CFD as a design and improvement tool. This tool can be used to improve pump performance and reliability in many different areas.

INTRODUCTION

Flow Related Problems in Pumps

Pump vibration, noise, cavitation and hydraulic performance problems are known to be related to and even caused by the

behavior of the fluid flowfield within the rotating and stationary passageways of the machine itself. Fluid/structure interactions that occur in high energy pumps are the reason that minimum flow limits are placed on these pumps by the manufacturers. While steady progress has been made in both reducing these limits and extending pump life, most of the effort to achieve these results has been experimental and, therefore, costly. Recent examples are a) the successive application of impeller outer diameter (OD) clearance gap alterations to the reduction of hydraulic instabilities connected mainly with the impeller-diffuser (or volute) interaction [1] and b) the technique of visualizing cavitating flow and making appropriate changes to the shape of the impeller blades that minimize or even eliminate cavitation [2, 3].

Computational Fluid Dynamics

With the objective of shortening pump development, design and upgrade projects, such work has more recently been accompanied by attempts to *compute* the complex flow fields involved. A similar, now time honored development in the computational area has been the finite element analysis (FEA) of stresses and vibratory behavior of machines and other structures. In fact, FEA is now required of pump OEMs by sophisticated users of highly stressed engineered equipment. In the not too distant future, the same can be expected to be true of the growing role of flow analysis in designing, applying and operating pumps. The increased computing power that is now available has made possible the development and commercialization of computer codes that, under quite reasonable assumptions, solve the classical Navier Stokes equations of fluid mechanics. Popularly known as "computational fluid dynamics" or "CFD," this technique is destined to take its place beside FEA in the storehouse of tools used by the average pump engineer today. Technologically astute pump users with demanding applications need to know about these advances in the art in order to avoid buying what to them would otherwise be a "black box." This in turn enables them to more intelligently procure, upgrade, operate, and maintain their equipment.

Quasi Three-Dimensional Analysis of Impellers and Diffusers

Impellers, as it turns out, have been more easily and effectively analyzed and, therefore, optimized than the stationary passages which convey the fluid to and from these rotating members. In the 1960s and 1970s, NASA and others developed axisymmetric flowfield codes that have served the turbomachinery industry well [4, 5]. Called "quasi three-dimensional" or "Q3D," because they use the convenient device of combining two-dimensional solutions of the flowfield to obtain results in the radial, axial, and circumferential directions within an impeller or other rotationally symmetric blade row, these codes are currently in use for designing highly engineered pumps with special demands relative to noise, cavitation, and life. However, the Q3D approach is limited, because it assumes the fluid to be flowing through a series of nested surfaces of revolution between the hub and shroud of an impeller. Yet, at flows near the BEP, Q3D yields reasonably accurate values of the main variables of interest in three dimensions, despite the fact that it cannot simulate a corkscrewing motion of the fluid within the passage. Also, as it does not employ a basic viscous flow formulation, Q3D is incapable of predicting the recirculating flow behavior and performance of a pump running at off-design, reduced flow conditions. To overcome these limitations, an objective of this paper is to gain the greater insight into impeller flows that is now possible with CFD.

CFD Analysis of Asymmetric Stationary Pump Flow Passages

Looking at the nonrotating passages of the pump, one finds, e.g., that a side suction approach passage to the impeller of a between-bearings pump cannot be analyzed with the Q3D restrictions. Coming from one part of the periphery of the pump, this passage requires truly three-dimensional methods that have had little application to such passages up to now. Yet the designer of a pump with a significant amount of head, namely a "high energy pump" (defined in [1]), needs to know how much nonuniformity and pressure loss this passage is creating in the flow that is entering the impeller. The same is true of many types of crossovers and other nonrotating passages found in multistage centrifugal pumps [6, 7]. Until quite recently, the only way to find out about these impeller entry flows has been to build models of the approach passages and pass air or water through them in the laboratory. An attempt to solve the flow in such a passage by truly three-dimensional methods was made with a new finite element CFD code on a boiler feed pump radial suction bay [8]. This code was utilized in a coarse grid so that the solution was essentially frictionless. This, however, was not far from correct, as the flow was accelerating in the converging passage—even though it had to make a turn into the axial direction to enter the impeller. Computed results agreed well with test results in air, and the circumferential distortions of the flow were obtained.

The commercial CFD code employed in the examples of this paper was utilized to compute the flow in the major portion of a multistage volute pump crossover [9]. Laboratory tests of the head loss in this crossover agreed well with that computed via the CFD code. More importantly, the computed solution revealed the characteristics of this flow, which is more complex and dominated by friction than in the suction bay, because a high speed flow enters the crossover from the upstream impeller and volute passage and has to diffuse rapidly to a much lower velocity, while executing a 180 degree bend back to the entrance eye of the downstream impeller. Substantially greater distortions occur in the flow, which in turn is ingested by that impeller.

This inlet distortion causes cyclic loading of the impeller blades, because they are then exposed to alternating angles of attack. At sufficiently high energy levels, this dynamic loading in turn produces noise and vibration that can adversely affect pump reliability. These fluid/structure interactions are exaggerated at off-design flows, thereby raising the minimum attainable flow rate and decreasing the runout capability. If distortions occur in the suction bay of the first stage, the fluctuating loading on the impeller blades produces lower local pressures and more cavitation within the impeller, thereby raising the NPSHR of the pump.

Improving Pump Design and Performance

Two cases are presented to illustrate the process of a) computing the flow, b) interpreting the results, and c) formulating improvements to the geometry, as a consequence of the insight gained in this interactive analysis/design process. The first is an impeller that was analyzed with the objective of ultimately improving operablility at minimum flow conditions, and the second is an analysis of the full multistage volute crossover mentioned above. The objective for this case was the introduction of design improvements that reduce the inevitable distortions and consequent losses and potential for vibration in higher energy pumping applications.

COMPUTATIONAL TECHNIQUE

CFD Software and Hardware Capabilities

Following two decades of research, several CFD computer codes are now available commercially. These all solve the Reynolds stress averaged Navier Stokes differential equations for viscous flow—most of them in three dimensions. All require mathematical modelling of the Reynolds stress terms in order to simulate turbulent flow. Some are now capable of computing flow in both stationary and rotating passageways through the inclusion of centrifugal and Coriolis terms in the equations. As with FEA

stress analysis, a flow passageway to be CFD analyzed must be divided up into many small elements, at the nodes of which corresponding values of the velocity magnitude and direction and the pressure are obtained. Large, complex passageways requiring much detail and incorporating the unsteady interactions of the flow in multiple blade rows require immense storage and computing capacity that is available only on Cray computers in central research establishments. The problems treated herein were restricted to steady flow through a single passageway and were solved on inhouse silicon graphics workstations using the CFD code TASCFLOW3D. This code has compared favorably with others applied to the same problems and against laser doppler velocimetry (LDV) test measurements of the actual flows [10]. Further, it has been shown to produce simulations of blade surface velocities that are equal to or better than those obtained via Q3D methods [11].

Steps in Obtaining the Solution

TASCFLOW3D is a "finite volume" based code, which uses a "k-epsilon" turbulence model and log-law wall functions to simulate the boundary layers. It is described in full detail in Thomas, et al. [12]. The flowfield is meshed in "blocks" as dictated by the local features of the passageway geometry, using a separately procured grid generation package. The computation is started with initial estimates of the velocity components and the pressure at every node. These values are continuously improved via up to one hundred or more iterative passes through the flowfield in which algebraic forms of the equations are solved at each node, until the amounts by which the equations are not satisfied (namely the "residuals") at these nodes are satisfactorily small. Variants of this approach are incorporated in the code that make for rapid convergence on accurate solutions in a reliable or "robust" manner.

Computing Time and Display of Results

For each case treated herein, CPU time varied from 24 to 48 hours, depending on the size of the mesh (number of nodes), utilizing a SGI Personal Iris 4D/35 workstation. This machine is rated at 6.3 million floating point operations per second (Mflops), a rate of computation that has already doubled in the new machines available as of this writing. Several weeks of effort were required to create each of the meshes that were required; however, future meshing of similar geometries is expected to consume much less effort. Automatic mesh generators are being developed that should reduce such tasks to a few hours.

The amount of data that is computed is so great that a full understanding and appreciation of the resulting flowfield requires an examination from several perspectives. The figures included herein give a few examples of the "post processing" ability of the computer code to meet this need. A further benefit of obtaining a CFD solution for the flow in a specific configuration is that one can store the data, come back to it later, and look at it from yet another perspective. This is particularly useful in becoming familiar with the three-dimensional vortical flow patterns that generally occur in typical pump flows, especially when recirculation is involved. If one were making experimental measurements of such a flow and needed this additional data, it would be necessary to set up and rerun the experiment, instrumented in accordance with the latest need to view the results from that fresh perspective!

IMPELLER RECIRCULATION

Pump and Test Loop Description

The first CFD application of this paper is the impeller of the 1500 specific speed (N_s) single stage end suction pump illustrated in Figure 1. This pump has a suction specific speed (N_{ss}) of approximately 13,000 and a BEP flow rate of 4525 gpm at 1785 rpm. This case was of interest, because it was desired to improve operation at minimum flow conditions. Because of the high N_{ss}, the impeller has a large eye relative to the exit diameter or OD; and this results in suction recirculation occurring at flowrates closer to the BEP than for lower N_{ss}. Sufficient NPSH to suppress significant cavitation exists at normal operating conditions so that this single phase CFD investigation properly applies.

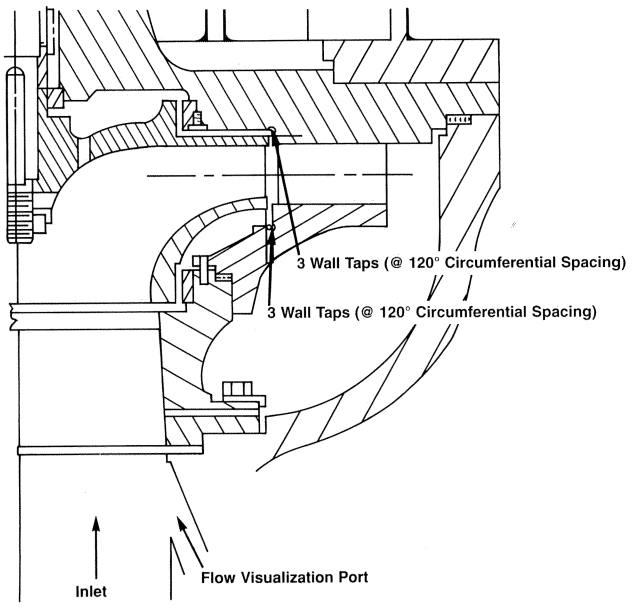

Figure 1. Pump Containing Impeller that was Analyzed and Tested. Flow is observed via optical ports and pressure measured at wall taps.

The entire CFD study of the impeller flow was accompanied by corroborating observations and measurements of the actual pump under test. The tests were conducted with the pump in the vertical configuration, and the vertical flow into the inlet eye of the impeller was quite uniform in comparison to that coming in from the radial inlet passageways of between-bearings pumps. The impeller inlet eye area could be seen through three optical ports (as indicated in Figure 1) while the pump was running, making it possible to observe and record strobed views of recirculating flow via video camera.

Six wall taps were used to measure the average static pressure downstream of the impeller, three on each side at the impeller OD. There were additional taps in the spaces between the impeller shrouds and the adjacent casing walls, which together with a strain-guaged coupling between the pump and drive motor, were employed to indicate the magnitude and direction of the static and dynamic axial thrust of the impeller.

The CFD Impeller Mesh

As indicated earlier, the first step in computing the flow via the code TASCFLOW3D was to create a suitable mesh or grid. This was done for one passageway of the impeller, which is what was analyzed. The intersections of this mesh with the impeller blade and hub surfaces is illustrated in Figure 2 for all five passageways combined. For clarity, the front shroud of the impeller has been omitted from this illustration. The mesh of the single passageway that was analyzed also incorporated blocks that extended the mesh both upstream and downstream of the impeller itself. This was necessary in order to be certain that recirculating flows at both inlet

and discharge would be included. Further, the boundaries had to be sufficiently far upstream and downstream, so as to be able realistically to apply the uniform or other boundary conditions required by the CFD code. With the extensions, the mesh of the single passageway contained 62,000 nodes.

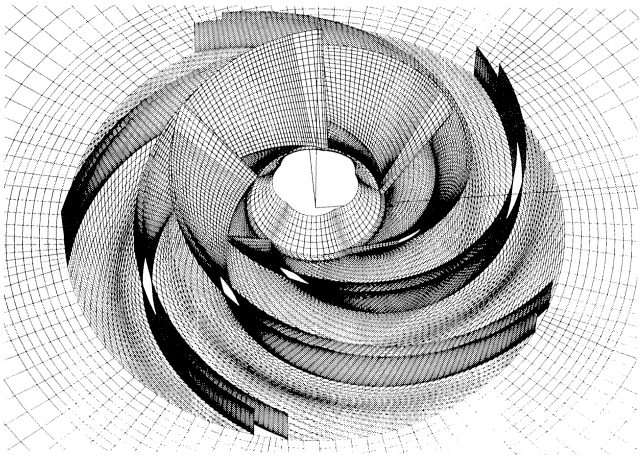

Figure 2. CFD Impeller Mesh. All five passages are shown; however, only one was analyzed. While the mesh spans the entire passage, only the intesections that it makes with the blade, hub, and shroud surfaces are illustrated.

This mesh was used for all the flowfield calculations, which were conducted at five flowrates from 105 percent down to 21 percent of BEP. The computation for each flowrate required about 70 iterations or passes through the mesh of the flowfield, which amounted to 24 hours of CPU run time.

Post processing the results for the first time consumed additional weeks of analysis, simply because it was necessary to take the time to decide how and where to access the solution to get illuminating and informative pictures, and to do the corresponding post processing that generates these pictures. Having established what to look at, it should not be necessary to spend more than a few hours of post processing time on similar configurations in the future.

Computed Results at Full Flow (105 percent of BEP)

The initial computation for the impeller was made at a flowrate that was 105 percent of that at the best efficiency point. Regardless of how the results were viewed, the flow was well ordered and showed no signs of significant slowing or reversal. An example is the depiction in Figure 3 of the velocity vectors near the suction side of the impeller blade. The greater the length of the arrows, the greater the velocity. It will be noticed that the direction of these vectors near the inlet is partly radial across the span or width of the blade—an indication of a centrifugal effect on the flow in the suction side boundary layer due to the blade shape in that region. Farther along in the passage, there is less radius difference across the span of the blade from hub to shroud; and there is then little indication of a radial component in the flow.

Computed Results at the Onset of Suction Recirculation

As the flow of the pump is reduced, the flowrate at which suction recirculation begins can be computed by approximate, empirical methods, that of Gopalakrishnan [13] being applicable here. The result for this pump is that suction recirculation is predicted to begin when the flowrate gets down to 67 percent of that at BEP [14]. The result of CFD computations at various flow points was

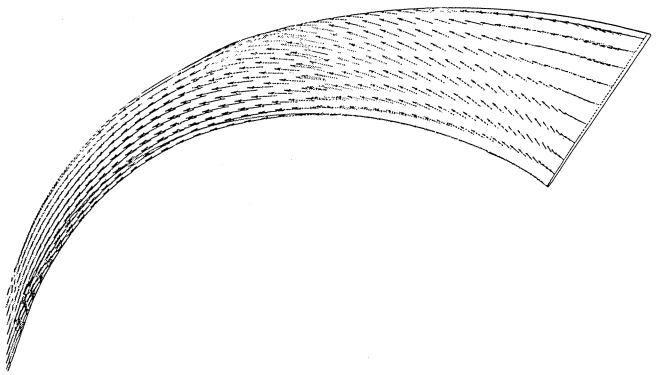

Figure 3. Impeller CFD Results at Full Flow. Relative velocity vectors are shown along the suction side of the blade at 105 percent of the BEP flowrate. The leading edge of the blade is on the right; the shroud surface of the blade is at the top of the figure; and the hub, at the bottom.

that suction recirculaton developed analytically at 71 percent of BEP, in reasonable agreement with the 67 percent predicted using the empirical formulation [13].

A view is presented in Figure 4 of the vectors near the front impeller shroud computed at 71 percent flow. Flow emerging from the pressure side is clearly flowing off the leading edge of the blade, the result of a stalled flow region that can be seen inside the passageway. The view is of the fluid motion relative to the blades, which means that since the blade is moving at velocity, U, so the absolute fluid velocity, V, is at least equal to U if not greater, at least in close proximity to the blade leading edge. Further, the major component of this flow is circumferential; i.e., recirculating fluid leaving the impeller is swirling in the direction of impeller rotation. However, such swirl is a small, local phenomenon until the flowrate gets low enough to cause significant recirculation activity upstream of the impeller.

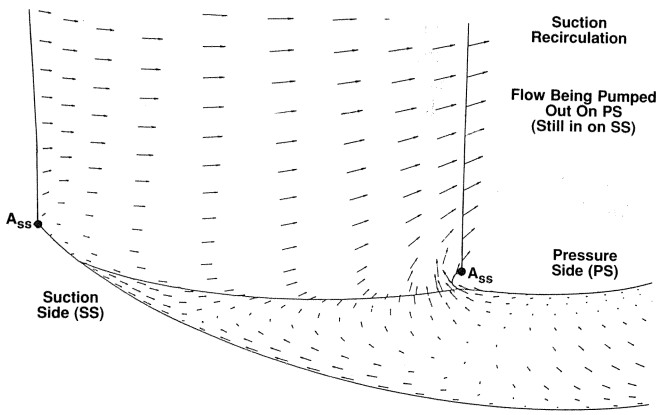

Figure 4. Backflow at the Impeller Blade Leading Edge. Flow pattern on the shroud surface of revolution at 71 percent of the BEP flowrate. The arrows indicate the local velocity relative to the passageway, which itself moves to the left.

The significant revelation via the CFD results at the above 71 percent onset flowrate is the recirculation vortex illustrated in Figure 5. Again, this is a view of the velocity vectors on the suction side of the impeller blade, but now a pair of dividing streamlines that meet in a saddle point B_{ss} at the shroud can be deduced, and these have been sketched onto the figure. Below this point a vortex

is produced that corresponds to the one reported by Schiavello [15]. This vortex is approximately perpendicular to the blade surface and very likely extends across to the pressure side of the passage. It is the result of viscous shearing between the incoming flow and the backflow, and there is a contribution coming from the fluid that is being pumped from the pressure side of the passage to the suction side as shown in the secondary flow pattern of Figure 6. At the saddle point of Figure 5, this flow coming from the pressure side is diverted upstream and downstream.

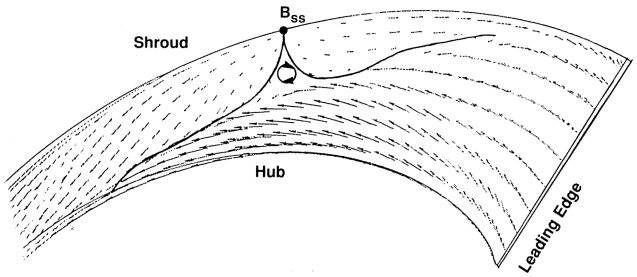

Figure 5. Recirculation Vortex Within Impeller. Flow pattern on the suction side of the blade at the onset of suction recirculation (71 percent of the BEP flowrate).

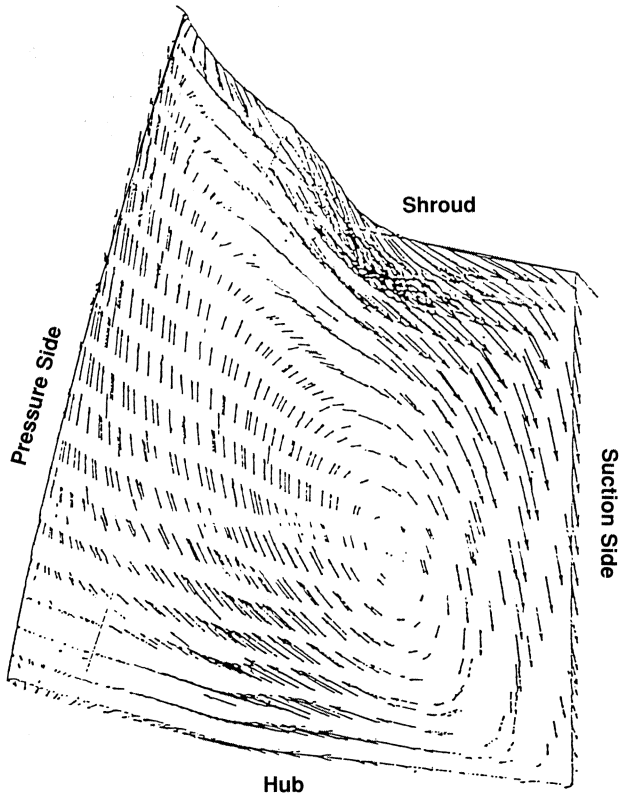

Figure 6. Secondary Flow Within Impeller. Projection of velocity vectors on a plane transverse to the primary relative flow direction—halfway through the passageway. Flowrate is 71 percent of that at BEP.

Computed Flows in Deep Suction Recirculation

Next, the flowrate was reduced further to 41 percent, and a CFD simulation of the widely observed upstream backflow that happens at these lower flowrates, i.e., in "deep suction recirculation," was produced and is illustrated in Figure 7. This is a meridional or radial cross section of the region upstream of the impeller blade leading edge, where the above mentioned swirling flow is fully developed, particularly at the shroud, because the fluid exiting the impeller is flowing upstream along the shroud. This highly swirling flow would naturally tend to flow outward if a passage were provided for it to do so; and this is why the backflow recirculator concept worked [16]. This is undoubtedly the first time that this well known flow pattern produced by the backflow phenomenon has been computed in detail by any method.

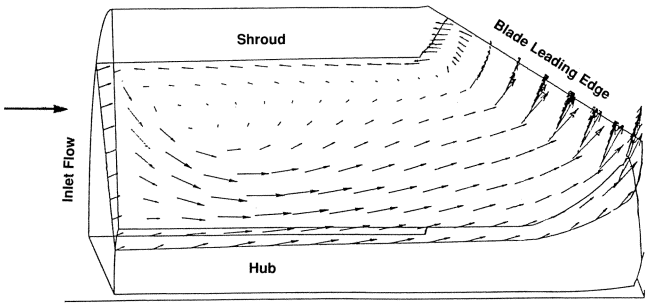

Figure 7. Recirculation Upstream of the Impeller. The stronger backflow occurring at 41 percent of the BEP flowrate extends well upstream of the impeller blade leading edge. The meridional velocity component of this strongly swirling flow is illustrated.

Occurrence and Computation of Discharge Recirculation

Impeller discharge recirculation in the test pump very likely occurs in conjunction with diffuser backflow, the fluid from both impeller and diffuser invading the spaces outside of the impeller shrouds where the leakage flow moves toward the impeller wear ring areas. This interaction causes a reversal, increase, and/or oscillation of the axial thrust forces acting on the impeller [1]. In the test pump of this study, a sudden increase in axial thrust occurred at 51 percent of BEP flowrate. Stalled flows at impeller discharge and in the space surrounding it were computed via CFD to begin at 42 percent of BEP. The higher flowrate of the tests could be due to the influence of diffuser backflow occurring at higher flowrates than would happen in the impeller alone, which is what was computed.

Computations were obtained at 21 percent of BEP flowrate, illustrating strong discharge recirculation. The results are shown in Figure 8, in which radial inflow can be seen at both hub and shroud—and radial outflow in the middle. The air testing done by Jaberg and Hergt [17] revealed a radial inflow at the front shroud at the impeller OD. Q3D equilibrium studies of the balance of flow elements between hub and shroud have shown that an appropriate blade twist at discharge will result in inflow at either side of the passage, hub or shroud. This combined with the kind of CFD viscous analysis being presented here should lead to inflow at both hub and shroud, as depicted in Figure 8.

Computation of Impeller Total Dynamic Head

A reasonable degree of confidence having been established in the ability of CFD to reproduce familiar occurrences regarding suction and discharge recirculation, it is natural to ask whether it can therefore predict pump total dynamic head TDH or, simply, total head H_t. First, the total head generated by the impeller was measured on test over the range from 105 percent down to 21 percent of BEP flowrate, with the help of the six wall taps illustrated in Figure 1. Then the CFD solutions over the same range were used to generate mass averaged total pressure results for the

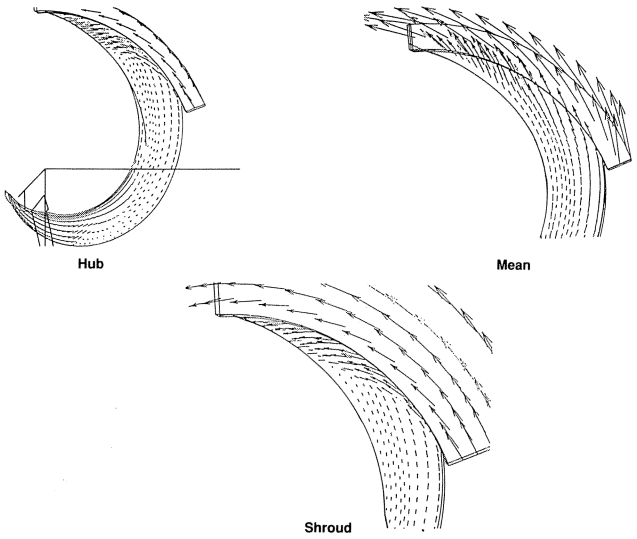

Figure 8. Impeller Discharge Recirculation. Flowrate is 21 percent of that at BEP. At the impeller OD, the flow is radially inward along both hub and shroud, while it is radially outward halfway between these surfaces. The arrows indicate velocity relative to the passage, which moves to the right (clockwise).

impeller at a radial station 13 percent of the impeller exit radius downstream of the impeller OD. The comparison of both test and computation is shown in Figure 9, in which the total head of the impeller is plotted. (Loss in the diffuser and collecting system of the pump would reduce this result somewhat.) The agreement is good, with the difference ranging from a five percent underprediction of head at the high end of the flow range to about a three percent overprediction at the lowest flowrate. The experimental uncertainty for the pump impeller total head is ±4 percent. In the future, it can be assumed that CFD will be used successfully to compute the head of the combined impeller and diffuser or volute. This would help to reveal droops, dips, and other head *vs* flowrate curve shape characteristics of interest to the user.

Impeller Design Improvements

The above CFD results led to a redesign of the impeller with a view toward reducing the minimum continuous stable flow. The approach was to reduce the flow rate at which the onset of suction and discharge recirculation occurs. This was done, first, by reducing the load on the blades, which produces early flow reversals and ultimately fully developed—and usually unsteady—recirculating flows at both suction and discharge. In the second place, patented leading edge shapes were added to the blades to further increase the range [2]. This new impeller is awaiting the testing needed to demonstrate the use of CFD as a tool in the process of improving the operability of pumps, whether they be in the field or new machines.

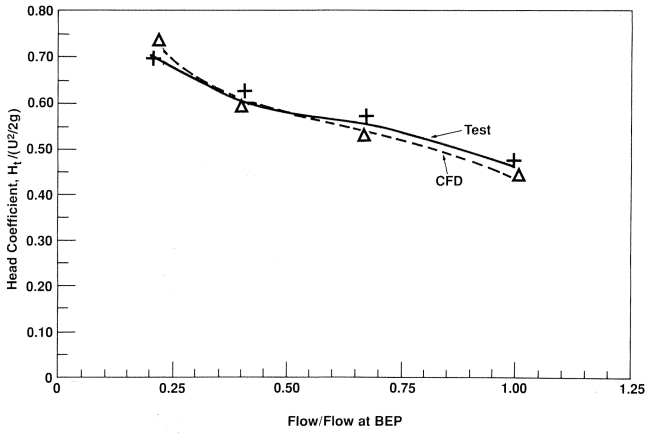

Figure 9. Impeller Total Head: Computed Vs Test. The CFD results compare favorably with those derived from measurements of static pressure at the impeller OD. Note that the head coefficient shown applies only to the impeller.

FLOW DISTORTION IN STATIONARY CROSSOVER PASSAGES

Multistage Volute Pump Crossover Description

Probably the most useful application of CFD for those involved with pumps is finding out the magnitude of flow nonuniformities that are created by asymmetric, stationary passageways that feed high head impellers. Relating these flow distortions to the severity of the response of the pump rotor is then necessary. Considerations of this kind have led to the well known guidelines for pump suction piping. However, in the case of multistage pumps, for the total pump package to be economical and rotordynamically satisfactory, the interstage passages cannot be designed according to such piping guidelines. A typical example is the diffusing crossover of Figure 10, which conducts fluid from the volute of one stage to the inlet eye of the next impeller. In this case, the horizontally split pump stages each have double volutes; so, one half, namely the upper crossover passageway, is depicted in Figure 10. The pump itself is of a 3×8 configuration (3.0 in discharge and 8.0 in impeller diameter) that handles 325 gpm (73.8 cubic meters per hour) at 3580 rpm. Each stage has a specific speed of 900 to 1000, depending on the diameter of the impeller cut. This multistage volute pump configuration is widely used, so that the results to be computed for this crossover are quite typical of similar equipment supplied by many OEMs today.

Computational Mesh for the Crossover

The core shown in Figure 10 is a negative of the actual passage shape; so, the wood takes the place of the fluid in the crossover. It can be seen that the fluid has to advance axially to the eye of the next impeller, shown at the lower right corner of the figure, while at the same time executing a 180 degree turn; i.e., the entering fluid is flowing upward from the lower left corner. In order to gain familiarity with the computational task for this highly three-dimensional geometry, just the 180 degree turn, without the final turn from radially inward to the axial direction, was first modelled and solved using the same CFD code employed here [9]. Now the complete passageway has been modelled, and the resulting mesh is illustrated in Figure 11. For clarity, just the intersections of this mesh with the boundaries of the passageway are shown. In reality, the mesh spans the entire internal volume of the crossover, the total grid containing 120,000 nodes, or twice the number needed for the impeller passageway. The computational time was correspondingly greater as well.

Several blocks of varying mesh orientation and spacing had to be constructed and combined to build the entire grid, including a downstream section that models the hub and shroud shapes of the next stage impeller. This added section was needed in order to establish the correct streamline shapes and resulting velocity distribution at the exit of the crossover, which in reality is the eye of the next impeller. The axial plane at this impeller eye, defined as the "P" plane in the inlet passage work of Silvaggio and Spring [18], is the plane of interest for seeing what kind of flow nonuniformities must be ingested by this next impeller. The "P" or eye plane is noted on Figure 11.

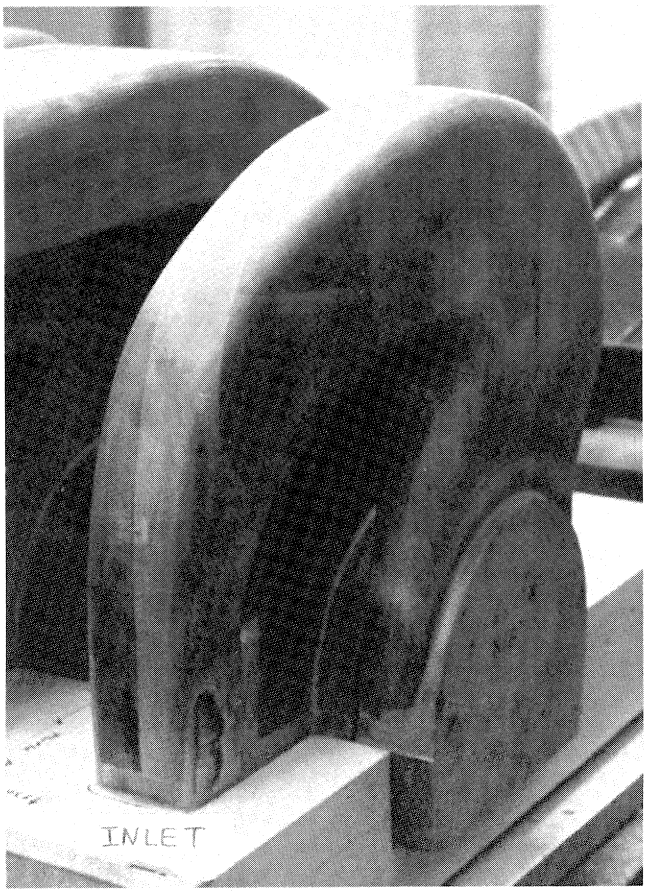

Figure 10. Foundry Core for Casting Crossover. The fluid emerging from one of the double volute halves surrounding the upstream impeller enters this top half of the crossover at the point marked "inlet" and is delivered to the eye of the downstream impeller at the lower right hand side of the photograph.

Computed Flow Patterns in the Baseline Crossover

The velocity vectors computed for the crossover are depicted along mesh lines in Figure 12. There are several surfaces on which to display such results; this one is the upstream side of the passageway, the side away from the viewer in Figure 10. It is the "outside" of the helical bend that moves the flow axially toward the next stage, while turning it 180 degrees in the plane of Figure 12. The side of the passage seen in Figure 10 has a different result; however, the main features of the flow can be seen in Figure 12 and in the velocity magnitude or "speed" contours of Figure 13. The fluid enters at the throat of the volute, which is at the lower right side in these figures, with no assumed swirl and diffuses to a lower velocity as it commences the 180 degrees turn. Here the flow separates from the inside of that turn and, in fact, backflow can be seen from the directions of the vectors. The fluid forms an active jet on the outside of the turn, which can be seen to result in prewhirling flow exiting the crossover into the eye of the next impeller at the left side of each figure. There, the inner diameter is that of the shaft going through the eye. On the right side of that exit area, a similar prewhirling flow can be seen coming from the lower half or bottom crossover that takes flow from the other half of the double volute surrounding the upstream impeller. As indicated in Figure 13, the flow in this passageway is characterized by a considerable range of velocity magnitude and direction. What matters most is how much of this variation remains when the fluid leaves the crossover at the next impeller eye.

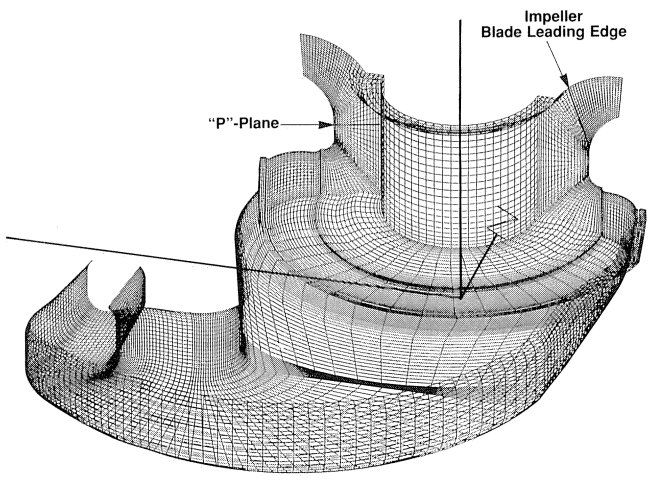

Figure 11. CFD Mesh for Full Crossover. Several "blocks" of the mesh are required for this highly three-dimensional geometry, which includes the hub and shroud of the downstream impeller.

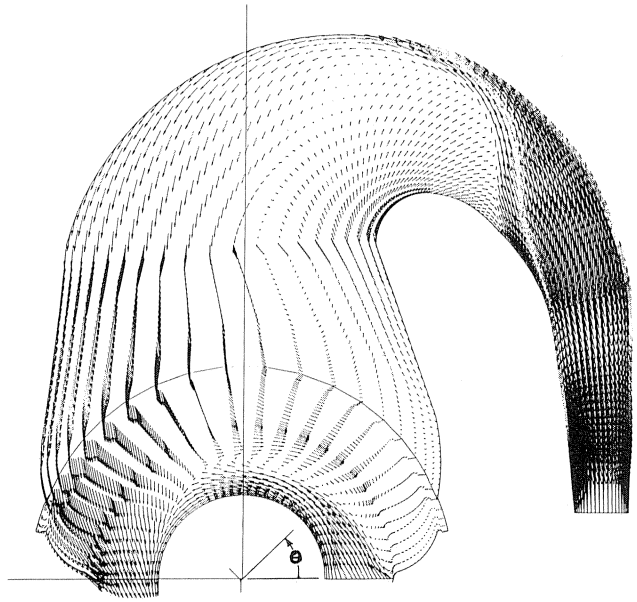

Figure 12. Computed Results for the Baseline Crossover. Velocity vectors are shown on the upstream side of the passageway, which is the outside of a helical turn that advances the fluid toward the downstream impeller. Rotation is counterclockwise.

Flow Distortion at the Eye of the Downstream Impeller

The velocity nonuniformities of Figure 13 are considerably reduced as the fluid accelerates into the eye of the next stage. This can be seen from the velocity contours of Figure 14, which have a range that is 2.5 times the one-dimensional axial velocity $V_{z,eye}$ through the eye; i.e., across the "P" plane. Plots in Figures 15 and 16 are representative, respectively, of the meridional or through-flow velocity V_m (essentially axial but with some radial component) and the circumferential or swirl component V_θ in the same plane. The circumferential or θ coordinate, which varies from zero to 180 degrees in these figures is defined on Figures 13 and 14. Obviously, the impeller blades will see different angles of attack

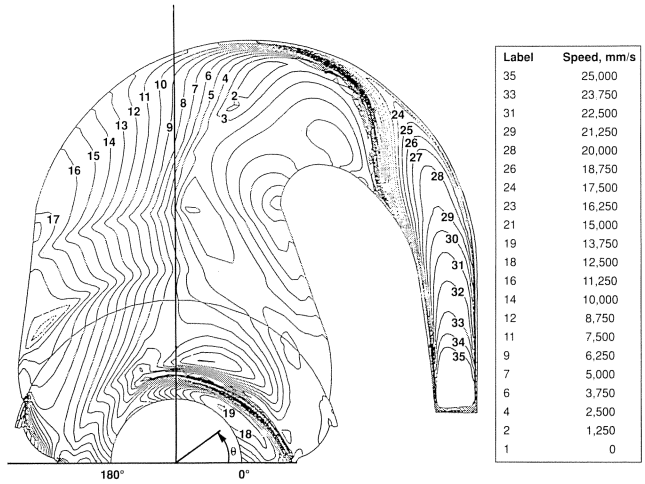

Label	Speed, mm/s
35	25,000
33	23,750
31	22,500
29	21,250
28	20,000
26	18,750
24	17,500
23	16,250
21	15,000
19	13,750
18	12,500
16	11,250
14	10,000
12	8,750
11	7,500
9	6,250
7	5,000
6	3,750
4	2,500
2	1,250
1	0

Figure 13. Constant Velocity Contours in the Crossover. Numbers on the contours denote velocity magnitude or "speed" in mm/s per the scale shown at the right. Regions of separated flow have extremely low velocity.

as they sweep through this varying field. The consequent incidence losses and varying lift on the blades arising from this distortion need to be evaluated, together with the accompanying pressure pulsations and related unsteady forces. A summary is presented in Table 1 of the distortions of both the total velocity magnitude and the two components of Figures 15 and 16. Approximate results for the maximum incidence angles on the blades of the next impeller are also given. Positive incidence occurs if the fluid strikes the pressure or invisible side of the impeller blade when looking into the eye. Reduced flowrates create more positive incidence; flowrates above that of the BEP create negative incidence—the fluid striking the suction or visible side of the blade.

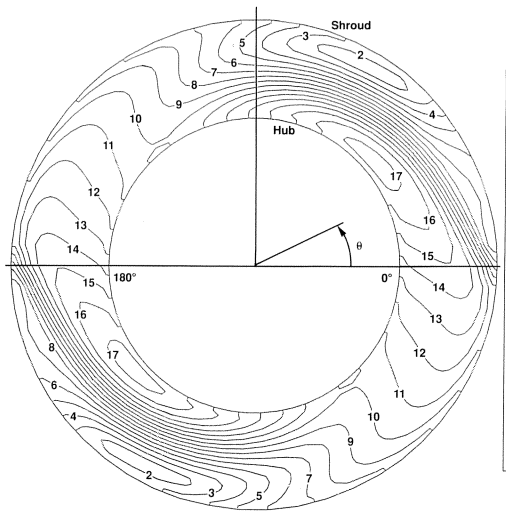

Label	Speed, mm/s
35	25,000
33	23,750
31	22,500
29	21,250
28	20,000
26	18,750
24	17,500
23	16,250
21	15,000
19	13,750
18	12,500
16	11,250
14	10,000
12	8,750
11	7,500
9	6,250
7	5,000
6	3,750
4	2,500
2	1,250
1	0

Figure 14. Flow Distortion at the Eye of the Downstream Impeller. Contours of constant velocity magnitude are found by the CFD post processor. A variation of 2.5 times the average axial velocity in the eye can be seen in this "P" plane.

Performance Effects

In the second half of Table 1 are listed the effects of the velocity variations listed in the first half. This information was obtained by

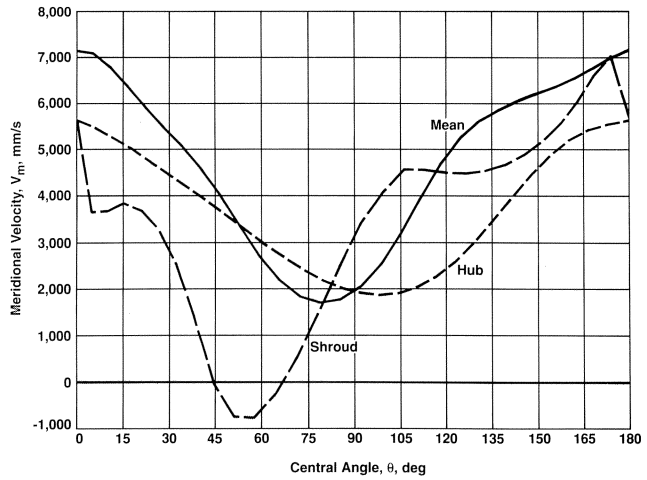

Figure 15. "Meridional" or Throughflow Velocity "V_m" at the Eye. These "P" plane results are shown for the 180 degrees of the crossover half as defined in Figures 13 and 14.

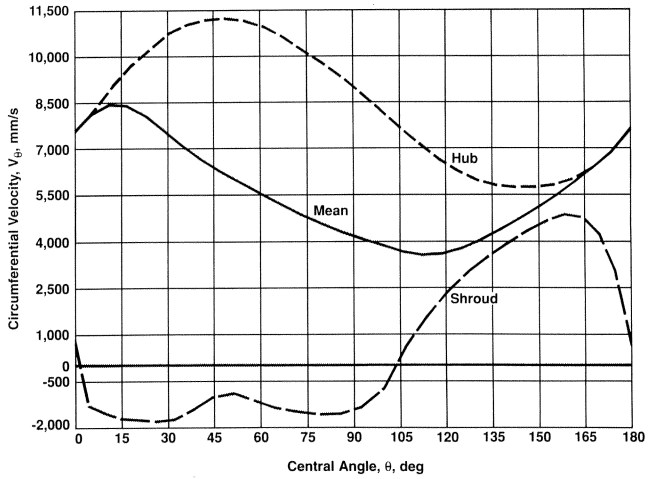

Figure 16. Circumferential or Swirl Velocity "V_θ" at the Eye. This and the throughflow given in Figure 15 are the two components of the total velocity vector in this plane.

recognizing that losses, lift and pressure pulsations are related to the inlet velocity relative to the impeller. For all practical purposes, this velocity is approximately equal to the local impeller blade speed at the inlet, essentially that of the maximum diameter of the eye rotating with the impeller, U_e. So, the losses are expressed as a loss coefficient multiplied by the corresponding velocity head $U_e^2/2g$. The greater the eye diameter, the greater this head is in comparison to the total head developed by a stage of the pump H_{stage}. The loss coefficient in turn depends on the incidence angle, and is usually small if the absolute value of that angle is less than 20 degrees; it increases rapidly outside of that range [19]. For the largest incidence shown, the loss coefficient is about 0.2; however, this large incidence is quite local. Assuming this condition to exist over no more than half of the flow in the peripheral direction and over only half the flow in hub-to-shroud annulus of the eye, the resulting value for the loss coefficient is effectively 0.05. This is the basis of the efficiency statements made in Table 1. Examination of the swirl in Figure 16 in a similar light yields the varying prewhirl or lift effect on H_{stage}. The local pressure pulsation is deemed to arise from the local loss coefficient (0.2 maximum).

Table 1. Flow Distortion in Multistage Volute Pump Crossover.

Velocity data at the "P" plane (impeller eye)	*Baseline*	*Splitter Vane*	*12 deg Swirl*
I. Velocity Variations			
$(V_{max} - V_{min})/V_{z,\,eye}$	2.5	1.3	1.8
$(V_{m,\,max} - V_{m,\,min})/V_{z,\,eye}$			
Shroud	1.8	0.6	0.7
Mean	0.9	0.7	0.8
Hub	1.3	0.5	0.7
$(V_{theta,\,max} - V_{theta,\,min})/V_{z,\,eye}$			
Shroud	1.5	1.4	1.5
Mean	1.1	0.8	1.0
Hub	1.3	1.1	1.9
Maximum incidence angle, deg			
Shroud	+20	+12	+13
Mean	-18	-10	-14
Hub	-41	-18	-23
II. Performance Effects			
Approximate efficiency change due to distortion, percentage points	-1.5	0	-0.2
Estimated efficiency gain over baseline, percentage points	----	0.5	1.3
Local prewhirl effect on head, Delta H/H_{stage}	+/-0.06	+/-0.06	+/-0.06
Local pressure pulsation due to distortion, Delta p/P_{stage}	0.06	0	0.01

So, for this baseline crossover, the approximate efficiency loss in the next impeller arising from the distortion in the eye as seen in Figures 14, 15, and 16 is 1.5 percentage points, and the consequent fluctuations in head and static pressure, p, are about six percent of the stage head and total pressure rise ΔP_{stage}. These are local effects and unless the stage head is much higher, as in high energy boiler feed pumps, the consequent load fluctuations will not produce destructive stresses in the pump structure. The efficiency loss could perhaps be improved, provided one does not propose a larger crossover passage that would destroy the compactness and economics of these popular multistage volute pumps.

Candidate Improvements

In the event that the crossover configuration considered here should be proposed for a high energy application, it would become more important to make improvements to reduce the distortion level of the baseline passageway. Simply studying the flow patterns revealed by the CFD results provides insight into what could be benificial changes to the geometry.

Splitter Vane

A fairly obvious step when viewing the flow in the 180 degree bend of Figure 12 is to insert a splitter or turning vane. This is quite easy mathematically, and such a vane is shown in Figure 17, for which the corresponding flowfield was computed. The vane simply follows the mesh, originating far up into the diffuser, to a point near the entry from the volute. This had a dramatic effect on the computed distortions, as can be seen in Figure 18 and Table 1. The throughflow velocity reversal reflected in Figure 15 for the baseline configuration is eliminated and the resulting distributions are quite uniform in comparison. The resulting incidence produces no loss; however, the friction drag on the vane (as found from testing to be described) cancels out much of the expected gain, yielding an estimated half point improvement. This friction loss would be less in a larger passageway. Furthermore, it is not generally practical to incorporate such a vane in a conventional casting the size of this example. The vane friction loss would, however, be less in a larger size passage; and the benefits of less distortion relative to vibration and pulsations still remain, regardless of the efficiency issue.

Swirl

Normally, an impeller centered in a volute produces two counter-rotating secondary vortices in the volute cross sections. Beneficial

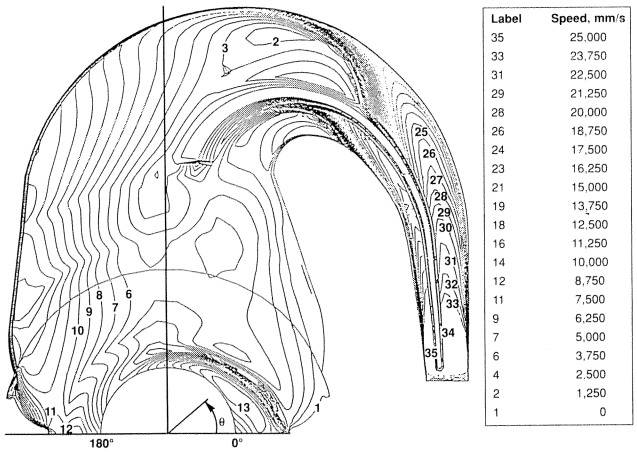

Figure 17. Flow Improvement Computed with Splitter Vane. These contours, in comparison to those for the baseline case (Figure 13) reveal smaller zones of separation, leading to less flow distortion at the eye of the downstream impeller. The splitter vane extends around the bend from the inlet to the crossover (which is on the right).

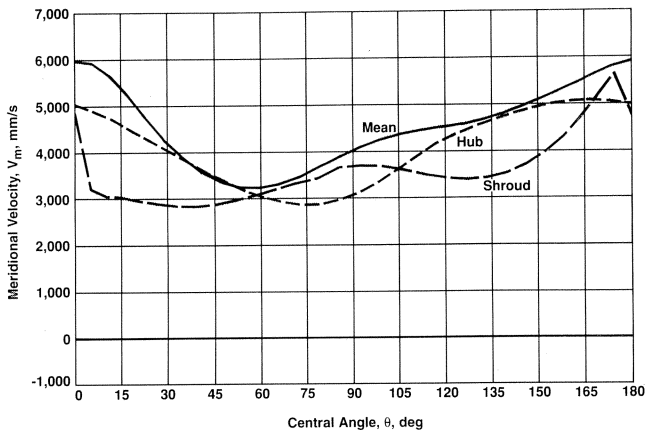

Figure 18. Throughflow at Eye for Computation with Splitter Vane. Note the improvement in uniformity of this meridional component of the velocity in comparison to the baseline case (Figure 15).

effects of this secondary volute flow on downstream diffusing and turning were assumed to be negligible for the baseline computation; therefore, no swirl pattern was imposed in the analysis on the flow entering the crossover passageway. On the other hand, it is commonly reported that a single swirl cell *is* beneficial; therefore, as a second idea for improving on the baseline results, a 12 degree swirl, again from testing [9], was imposed at the volute throat or entrance to the crossover. The sense of the swirl was clockwise as viewed from upstream of the entrance. Such a swirl cell could be created by moving the impeller back, i.e., away from the suction. However, changes in the shape of the volute cross section would probably also be needed. The results are summarized in Table 1, the corresponding "P" plane throughflow distributions being shown in Figure 19. If this swirl could be realized, the efficiency gain associated with the improved flow pattern at the impeller inlet is predicted to be 1.3 percentage points. The pressure pulsations are predicted to be much smaller than for the baseline case.

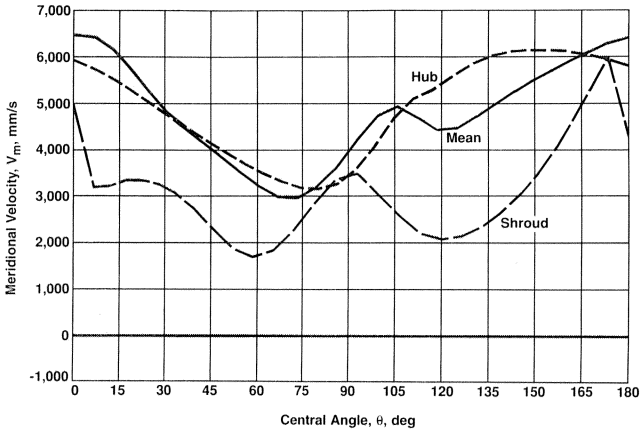

Figure 19. Throughflow at Eye Computed with 12 Degree Inlet Swirl. Swirl in the entering flow aids the turning of the flow in the crossover and reduces the distortion at the eye in comparison to the baseline case of Figure 15.

Preswirl Results

Neither of these improvements changed the basically sinusoidal character of the swirl component (Figure 16), as this is primarily a function of the shape of the outer walls of the crossover as it approaches the eye. Fluid entering at the shroud (OD of the eye or "P" plane) on the right side of the eye in Figure 12 is necessarily swirling opposite to the direction of rotation of the impeller, which is counterclockwise in that figure (clockwise in Figure 10). It swirls *in* the direction of rotation on the left side of the figure. For this reason, the effect of the prewhirl on pump head is the same for all the cases of Table 1. Nevertheless, these two candidate improvements are an indication of the value of CFD in a) providing the insight needed to make improvements, and b) evaluating the ideas that are proposed.

Verification Testing of Crossovers

As described by Graf, et al [9], the 3 × 8 multistage volute pump crossover that is a subject of this discussion was bench tested in accordance with the schematic diagram of Figure 20. A photograph of the test setup is shown as Figure 21. Both halves of the crossover had to be included in order to produce the correct exit flowfield. (In the CFD work, the effect of the opposite crossover half was included by mathematically imposing symmetry conditions on the non-wall exit boundaries of the mesh.) Water was introduced in equal amounts at the two volute throat entry points,

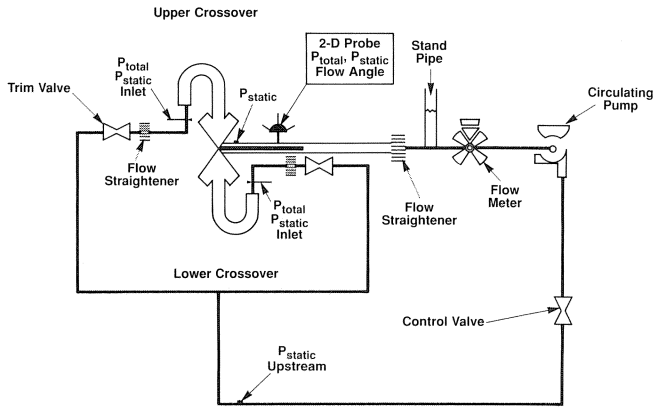

Figure 20. Test Setup Schematic for the Crossover. Both halves of the multistage double volute pump crossover were tested in water as indicated in this diagram.

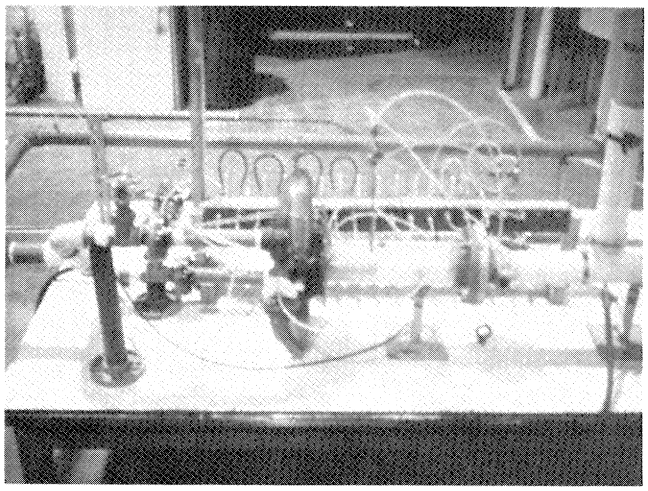

Figure 21. Photograph of Crossover Test Setup. Transparent, full size crossover passages were tested.

and pressure measurements were made to assess performance effects of turning vanes and swirl.

As stated above, as long as the basic channel geometry was unchanged, the introduction of vanes anywhere in the passageway produced essentially no efficiency improvements. Distortion was not measured, and the downstream pressure that was measured was a result of the mixing out of the distorted flow that had existed at the eye or "P" plane. In the CFD work of Graf, et al. [9], a simplified version of the exit from the crossover was employed in which the flow was accelerated in order to minimize the influence of anything other than the actual exit geometry on the upstream flow of interest. Thus, the distortions were analytically mixed out at the exit of that crossover. Very good agreement between the measured pressure recovery and those CFD results were obtained. For the present work, with the actual exiting flow not mixing out prior to entering the next impeller, the mixed-out pressure recovery data shown in Figure 22 were taken as a reasonable indication of optimum swirl to use in the 12 degree swirl computations described earlier.

CFD BENEFITS TO THE USER

Having demonstrated the validity of CFD and the insights afforded to the designer from CFD solutions of pump hydraulic

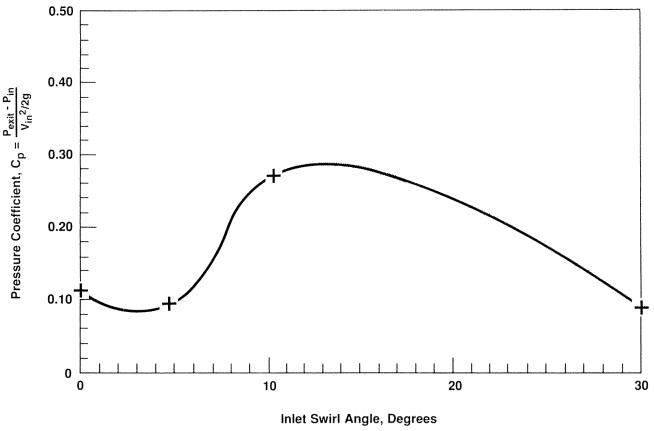

Figure 22. Crossover Pressure Recovery Vs *Swirl Angle. The optimum angle of the inlet swirl was found to be approximately 12 degrees on test.*

components, it is now appropriate to point out the potential applications of this tool for meeting user needs. Most of these applications stem from a) reduction of flow distortion in suction bays and crossovers, and b) reduction of local velocity decelerations within impellers, and may be summarized as follows:

- NPSH-margin reduction—less local cavity blockage, arises in impeller when excessive and fluctuating angles of attack of flow onto blades are reduced by establishing more uniform approach flows.

- Rangeability broadening (lower minimum flow; higher runout)—less flow distortion produces less vibration at low flow.

- Reliability enhancement through vibration reduction—less flow distortion reduces fluctuating load on structure.

- Impeller life extension through cavitation reduction—less excursion in angle of attack shortens the average length of cavities streaming off blade leading edges, which in turn decreases the resulting cavitation erosion.

- Efficiency upgrade—incidence losses decrease when angles of attack are reduced.

- Trouble shooting help—flow-related causes of vibration are identified and eliminated.

In all these cases, the cost and time of running CFD solutions that identify potential problem areas and verify design improvements is less than building and testing a model—especially when geometries are involved that are similar to what has been analyzed earlier—i.e., impellers, inlets and crossover passages. Furthermore, the analysis can produce a wider range of displays of the flow that would be much more time consuming to develop from test data than to obtain by querying the CFD solution and computer-plotting the results. Such displays provide the insight needed to make design improvements that might otherwise remain obscure and untried.

CONCLUSIONS

A commercial three-dimensional viscous flow computer code has been applied to both rotating and stationary members of pumps, with a view to understanding the flow well enough to make improvements leading to smoother, more efficient operation. Called TASCFLOW3D, this code solves the Navier Stokes equations in a finite volume mesh on a currently available workstation. Two problems were solved, one an impeller with 62,000 nodes and the other a multistage volute pump crossover with 120,000 nodes. Computation time for a given flow case was 24 to 48 hr, depending on mesh size. The calculation method is called computational fluid dynamics (CFD) analysis.

The impeller is from a 1500 specific speed, 4525 gpm, 1785 rpm end suction pump having a suction specific speed of 13,000. Suction recirculation flow patterns were computed for the first time, and the results agreed very well with experimental observations, including the vortical behavior that develops within and upstream of the impeller. Discharge recirculation was computed to occur at 42 percent of BEP flowrate—somewhat below the experimentally obtained result of 51 percent. This difference is attributed to the influence of diffuser backflow in the test pump, which was not calculated via CFD. The impeller total head curve computed via CFD agreed with test measurements within five percent. As a result of the insight gained from the analysis, a new impeller has been designed to improve operability and reliability at minimum flow conditions. This is a commercial pump that is presently awaiting test.

The crossover is the primary stationary flow passage of a 325 gpm, 3580 rpm, 3 × 8 multistage volute pump with 900 to 1000 stage specific speed. This passage diffuses the flow emerging from the volute of the upstream stage and turns it through a 180 degree bend as it also moves the fluid axially and out into the eye of the downstream impeller. The resulting distortions of the velocity field entering this impeller were computed to be 2.5 times the average eye throughflow velocity. This is estimated to cost about 1.5 percentage points of efficiency on the performance of the next stage. Improvements were then analyzed, which illustrate the utility of CFD as a tool to improve existing pumps or to develop new designs. One of these improvements was a turning vane inside each crossover half that halved the computed flow distortion, and the other was the introduction of swirl at the inlet to the crossover from the volute, which yielded a lesser but acceptable reduction of distortion while predicting a 1.3 percentage points of efficiency improvement. While the distortion does not create an operational problem for the pump analyzed, it could, if not corrected, produce vibratory response of a high energy application of the pump and surrounding structure.

CFD has enabled those who use it, both for pump design and for other flow problems encountered in user installations, first, to break out of the syndrome that requires an experiment to answer questions about flowfields. Secondly, it opens the way for the cost effective improvement of pump hydraulic elements that is possible when offending flow patterns can be identified and then eliminated by otherwise undiscoverable design alterations. Finally, it is to be expected that CFD analysis will come to be accepted to the degree that finite element stress analysis (FEA) is currently regarded by many users of complex, highly stressed equipment. In fact, users of such equipment routinely specify FEA in their contracts with suppliers. There is every reason to believe that CFD will eventually play a similar role in the sphere of fluid flow in pumps and other equipment.

REFERENCES

1. Cooper, P., Wotring, T., Makay, E., and Corsi, L. "Minimum Continuous Stable Flow in Feed Pumps," *Symposium Proceedings:Power Plant Pumps*, EPRI CS-5857, pp. 2-97 to 2-132 (1988).
2. Sloteman, D. P., Cooper, P., and Graf, E., "Design of High-Energy Pump Impellers to Avoid Cavitation Instabilities and Damage," *Power Plant Pumps Symposium*,Tampa, Florida, EPRI (June 1991).
3. Cooper, P., Sloteman, D. P., Graf, E., and Vlaming, D. J., "Elimination of Cavitation-Related Instabilities and Damage in High-Energy Pump Impellers," *Proceedings of the Eighth*

International Pump Users Symposium," The Turbomachinery Laboratory, Texas A&M University, College Station, Texas (1991).

4. Katsanis, T. and McNally, W. D., "Revised Fortran Program for Calculating Velocities and Streamlines on the Hub-Shroud Surface of an Axial-, Radial-, or Mixed-Flow Turbomachine or Annular Duct," NASA TN D-8430 (1977).
5. Katsanis, T. and McNally, W. D., "Revised Fortran Program for Calculating Velocities and Streamlines on a Blade-to-Blade Surface of a Turbomachine," NASA TM X-1764 (1969).
6. Return Passages of Multistage Turbomachinery, FED, *3*, ASME (June 1983).
7. Flow in Primary, Nonrotating Passages in Turbomachines, ASME (December 1979).
8. Dhaubhadel, M. N., Akay, H. U., Singh, P. J., Spring, H., and Prescott, M., "Three-Dimensional Finite Element Analysis of Flow Through a Double Suction Pump Bay," Pumping Machinery - 1989, FED, *81*, ASME (1989).
9. Graf, E., Sloteman, D. P., Singh, P., and Raw, M. J., "Three-Dimensional Flow Analysis in a Multistage Pump Crossover Diffuser," Fluid Machinery Components, FED, *101*, ASME (1990).
10. Schachenmann, A., Muggli, F., and Guelich, J. F., "Comparison of Three Navier-Stokes Codes With LDA-Measurements on an Industrial Radial Pump Impeller," Pumping Machinery - 1993, FED, *154*, ASME (June 1993).
11. Graf, E., "Analysis of Centrifugal Impeller BEP and Recirculating Flows:Comparison of Quasi-3D and Navier-Stokes Solutions," Pumping Machinery - 1993, FED, *154*, ASME (June 1993).
12. Thomas, M. E., Shimp, N. R., Raw, M. J., Galpin, P. F., and Raithby, G. D., "The Development of an Effficient Turbomachinery CFD Analysis Procedure," *Proceedings of the 25th Joint Propulsion Conference,* sponsored by AIAA, ASME, SAE and ASEE in Monterey, AIAA-89-2394 (1989).
13. Gopalakrishnan, S., "A New Method for Computing Minimum Flow," *Proceedings of the Fifth International Pump Users Symposium*, The Turbomachinery Laboratory, Texas A&M University, College Station, Texas (1988).
14. Graf, E., "Suction and Discharge Recirculation Patterns in a Centrifugal Pump Impeller," Proceedings of ROCON '93, sponsored by New Jersey Institute of Technology and ASME, Newark, New Jersey (1993).
15. Schiavello, B., "Cavitation and Recirculation Troubleshooting Methodology," *Proceedings of the Tenth International Pump Users Symposium*, The Turbomachinery Laboratory, Texas A&M University, College Station, Texas (1993).
16. Sloteman, D. P., Cooper, P., and Dussourd, J. L., "Control of Backflow at the Inlets of Centrifugal Pumps and Inducers," *Proceedings of the First International Pump Symposium*, The Turbomachinery Laboratory, Texas A&M University, College Station, Texas (1984).
17. Jaberg, H. and Hergt, P., "Flow Patterns at Exit of Radial Impellers at Part Load and Their Relation to Head Curve Stability," Pumping Machinery - 1989, FED, *81*, ASME (1989).
18. Silvaggio, J. A., Jr. and Spring, H., "Air Model Testing to Determine Entrance Flow Fields," *Proceedings of the First International Pump Symposium*, The Turbomachinery Laboratory, Texas A&M University, College Station, Texas (1984).
19. Hawthorne, W. R., *Aerodynamics of Turbines and Compressors*, Princeton University Press, p. 280 (1964).

ACKNOWLEDGEMENTS

The authors extend their appreciation to the following persons within the Ingersoll-Dresser Pump Company: Donald P. Sloteman, Kim Horten and Michael Adams, who obtained the experimental data that were used to assess the validity of the computational results of this paper; Charles Heald, John Eyen, and William Ord, who provided the necessary support for this work; and Ian P. Massey, whose vision and ongoing support have given us much encouragement in this relatively new area for the commercial pump field.